Atomic Force Microscopy-Based Static Plowing Lithography Using $CaCO_3$ Nanoparticle Resist Layers as a Substrate-Flexible Selective Metal Deposition Resist

Authors: Sasanka B. Ulapane,[†] Jennifer L. Doolin, [†] Monisola K. Okeowo, [†] Cindy L. Berrie[†*]

[†]Department of Chemistry, University of Kansas, Lawrence, Kansas 66045

[*]Corresponding author: cberrie@ku.edu

Abstract

Atomic force microscope (AFM) tip-based fabrication has gained attention due to its unparalleled precision and control for designing nano- and microscale features. Such features have utility in applications including miniaturized electronics, biological sensing, and plasmonics. Herein, we discuss an AFM tip-based plowing approach to create patterns on the micron scale in a thin $CaCO_3$ nanoparticle film, deposited over a wide range of substrates. The $CaCO_3$ nanoparticle layer's high thermal stability allows it to be used as a resist film during high vacuum thermal evaporation of gold. After metal deposition, the nanoparticle resist film is selectively removed in aqueous solutions either by complexing with ethylenediaminetetraacetic acid (EDTA) or dissolution with dilute HCl. The resulting gold metal features on surfaces were characterized by AFM and optical microscopy. The metal features were commensurate with the patterns created in the nanoparticle film. This fabrication approach was demonstrated on glass, Si, and mica and the metal features show reasonable adhesion and stability. This patterning approach is unique in that it allows the deposition of precisely placed metal microstructures with defined size, shape, placement, and orientation on various substrates while using simple, easily removeable resists. Salt-based resists can be removed in aqueous solutions with minimal contamination or damage to

metal features. This versatile method could be used to deposit fixed metal features on any desired substrate for applications from sensors to electronics. This is particularly useful for applications with conductive structures on optically transparent substrates, which are more challenging to fabricate with other approaches.

Introduction

In recent years, the fabrication and miniaturization of metallic structures has drawn a lot of attention as the demand for smaller electronic devices and the need to conserve expensive metals increases. Nanomaterials are useful for many different applications, such as: miniaturized electronics,[1] biological[2] and plasmonic[3-6] sensing devices, surface enhanced Raman spectroscopy (SERS),[7] solar energy applications,[8,9-12] photodetectors,[13] and catalysis.[14-17] The properties of metallic nanostructures are highly dependent on their chemical identity, size, and shape. Solution-based synthesis of metallic nanoparticles provides well-defined control over the nanostructures' size and shape,[18-19] but lacks the ability to control their placement on a surface. Versatile techniques are required to manufacture small metallic structures with controlled shape and orientation on different substrates.

Metal can be deposited on a surface using various techniques such as electrolysis (also known as electroplating),[20] electroless deposition,[21-22] atomic layer deposition (ALD),[23] electron beam deposition,[24] sputter coating,[25] and thermal evaporation.[26] On a bare substrate, these techniques deposit metal over the entire surface. Resist layers can be deposited over the surface and patterned, before metal deposition, to ultimately form defined metal structures on a surface. Where there is resist material, metal is blocked from interacting with the substrate. The resist layer can be removed after metal deposition, leaving the desired metal feature behind on the surface.

Organic materials (including both polymers and self-assembled monolayer (SAM) films) are routinely used as resist films. Some organic molecules can spontaneously form self-assembled monolayers (SAMs) on substrates. The head-group of a molecule chemisorbs to a specific substrate, while intermolecular interactions stabilize the tails, so the molecules stand in an upright orientation on the substrate.[27] This spontaneous process stops once the substrate is covered, therefore SAMs are only one molecule thick.[27] The formation of SAMs requires specific molecule-substrate chemistry. For example, thiol-based molecules specifically bind with metal surfaces[28-30] and silane-based molecules bind to silicon substrates.[31-32] Polymer thin films are also used in nanostructure fabrication.[33-36] Unlike SAMs, organic polymers do not require specific chemistry to bind to a surface; they can be deposited through solvent deposition and subsequent spin-coating.[35, 37]

In order to function as a resist, some of the resist layer must be removed to expose the underlying substrate for metal deposition. Several techniques have been developed to control the orientation and shape of metal structures on surfaces. Top-down fabrication techniques, such as stencil lithography (also known as shadow mask deposition),[38-39] microcontact printing,[40] and imprint lithography,[41-43] create well-defined metallic structures at an industrially feasible throughput,[44-45] but are limited to creating features with lateral dimensions of more than a hundred nanometers. Electron- or ion-beam lithography can make nanometer-sized features but requires expensive equipment.[46-47] Bottom-up fabrication techniques allow for the growth of smaller metal features. Particle lithography methods are an efficient way to pattern large areas of organic resist layers, but the size and shape and the resulting metallic nanostructures are limited by the shape and spacing of the particles.[48]

Scanning probe microscopy (SPM)-based fabrication techniques, while lacking throughput, allow for precise control over the location and shape of extremely small features with dimensions from several nanometers to microns in dimension. Tip-based methods have been demonstrated in several fabrication approaches including dip-pen nanolithography (DPN),[49-53] local anodic oxidation,[54-56] thermochemical/chemical nanolithography,[57-59] electrostatic nanolithography,[60] and static plowing lithography.[35, 61] In addition, atomic scale manipulation,[62] as well as orientational arrangement of metallic nanowires,[63] has been demonstrated.

Static plowing lithography, also referred to as "scratching" and "nanoshaving", is a common, AFM-based method used to remove an area of a resist layer, thereby exposing the underlying substrate. The AFM probe is brought into contact with the surface, and enough pressure is applied to the tip to physically, and selectively, remove some of the resist layer.[35, 61, 64] This method is compatible with many substrates[45, 65] and its resolution is ultimately limited by the AFM radius of curvature of the probe tip. Static plowing lithography has been used to selectively remove areas of resist layers composed of SAMs,[64, 66-67] polymers,[35-36] or thin sheets of ice.[68] While each of these resists have applicability on particular substrates, or under particular conditions, they all have some limitations (e.g., SAMs can only form on specific substrates, ice films can only be patterned at low temperatures). Using static plowing lithography, in conjunction with a resist layer, allows one to control the placement, size, and shape of metal features grown on the surface.[67] However, addressing issues like choosing an easily removable resist film (for contamination free substrates upon completion) with excellent patternability and applicability on a range of surfaces,[64] rapid wearing of AFM probe tips,[64] are still active areas of research.

While organic-based resist layers have been used as templates for metallic nanostructure growth in solution, they do present some challenges. SAM formation requires specific molecule-

substrate chemistry, so SAMs cannot be formed on arbitrary materials. It is also difficult to remove the organic material after metal deposition. SAM removal with solution-based methods requires exposure to harsh reagents[69-70] that can damage the metal nanostructures.[71] Furthermore, organic resist layers are not suitable for every metal deposition method. Atomic layer deposition (ALD) and thermal evaporation require elevated temperatures and vacuum environments[23] that could cause decomposition of organic molecules.

We are interested in developing a novel resist layer that can be applied to many types of substrates, withstand high-temperature metal deposition conditions, and be removed easily leaving the metal nanostructures intact. Salts are interesting candidates for several reasons. First, they are common and relatively inexpensive. Second, they can be deposited on any substrate; no specific surface chemistry is required for salts to adhere on a surface through physisorption. Third: salts have very high melting points and can withstand the high temperatures required for ALD. Finally: solution conditions can be tuned to remove salts without damaging the desired metal features.

In this work, we report using $CaCO_3$ nanoparticles as a novel, versatile, and robust resist layer that can be used on many different substrates. Static plowing lithography is used to create microscale patterns in the $CaCO_3$ resist layer. We varied the nanoparticle preparation method, nanoparticle surface coverage, static plowing lithography scanning parameters, and substrate to optimize pattern formation on multiple substrates. After patterning, a gold metal was thermally evaporated onto the samples. Then the $CaCO_3$ resist layer, and excess metal, were cleanly removed from the surface by reactions with dilute hydrochloric acid (HCl) or Ca^{2+} chelating agents, resulting in isolated metal microstructures. We demonstrated that salt-based resist layers are a viable, robust resist layer that increase the versatility of bottom-up manufacturing of metallic features with controlled orientation, placement, and size on a range of substrates.

Materials and Methods

Materials

Ethylenediaminetetraacetic acid (EDTA), Calcium nitrate tetrahydrate ($Ca(NO_3)_2 \cdot 4H_2O$), Sodium nitrate ($NaNO_3$), Triton X-100 (4-(1,1,3,3-Tetramethylbutyl)phenyl-polyethylene glycol), and commercial $CaCO_3$ powder were purchased from Millipore Sigma (St. Louis MO). Anhydrous sodium carbonate (Na_2CO_3), ACS grade sulfuric acid (H_2SO_4), 30 % hydrogen peroxide, and hydrochloric acid (HCl) were purchased from Fisher Scientific (Waltham, MA). Sodium hydroxide (NaOH) was purchased from Baker Analyzed Reagents (Phillipsburg NJ). 99.999% pure Au shots or wires for thermal evaporation were purchased from Alpha Aesar (Haverhill, MA). Precleaned microscope slides (from Fisher) $25\ mm \times 75\ mm \times 1.9\ mm$ were used as glass substrates. Single-side polished Si (100) wafers were purchased from Virginia Semiconductor (Frederickesburg VA). Ruby Muscovite Mica was purchased from Lawrence Mica Company. Reprorubber Thin Pour 130 ml Kit was purchased from Penn Tool Co. (Maplewood, NJ) to mount samples on AFM pucks.

Surface Preparation

Approximately 1×1 cm^2 pieces of mica, silicon, and glass substrates were used in this study. Mica surfaces were cleaved immediately prior to use to expose a clean, uniform surface. Glass and silicon substrates were piranha cleaned at ~60-80°C in a 3:7 mixture of 30% H_2O_2 and concentrated H_2SO_4 for 20 min. (*Piranha solution is extremely corrosive, potentially explosive, if capped in a sealed container, and must be handled with caution. Proper personal protective equipment must be worn at all times during the preparation and handling of the piranha solution. The piranha solution should be properly disposed of immediately after use).* Following piranha

cleaning, the substrates were thoroughly rinsed with deionized water and dried with a stream of N_2 gas.

$CaCO_3$ Nanoparticle Synthesis

$CaCO_3$ nanoparticles were prepared by a protocol slightly modified from previous reports.[72-75] Briefly, 40 mL of a 0.20 M aqueous solution of $Ca(NO_3)_2$ was mixed dropwise with 100 mL of an aqueous solution of 0.18 M $NaNO_3$, 0.20 M NaOH, 0.10 M Na_2CO_3, and 250 µL of neat triton-x (final concentration approximately 3 mM) while stirring vigorously. The rate of addition of the $Ca(NO_3)_2$ solution was approximately 3 mL/min. Once the nanoparticles were formed, they were filtered out of solution using a Buckner funnel and were thoroughly rinsed with deionized water. The nanoparticles were dried at 120˚C for 1 h, then mechanically separated by grinding to a powder using mortar and pestle before storing. A similar protocol was used for preparation of $BaCO_3$ particles (see SI for details).

To disperse the nanoparticles in water for depositing on surfaces, 0.10 g of the nanoparticle precipitate was added to 5.0 mL of deionized water. The resulting suspension was sonicated for 30 min to ensure dispersion of aggregated nanoparticle clusters. This stock suspension was diluted to desired concentrations. Aliquots of either 50 or 100 µL of each diluted nanoparticle suspension were deposited onto the desired surface (glass/mica/Si) and allowed to dry for 2 h under ambient conditions. Once the samples were completely dry and formed an even film, they were mounted on AFM pucks with RePro Rubber for patterning. This allows the samples to be easily removed from the AFM mounts for metal coating with minimal disturbance or contamination.

AFM Micropatterning

The nanoparticle resist film was selectively removed using diamond-like carbon (DLC) coated Tap300DLC probes (Budget Sensors k ~ 40 N/m and f ~ 300 kHz) to fabricate the desired

patterns on each surface. Patterning parameters (including tip velocity, applied load, and number of passes over the pattern) were varied to find optimal patterning parameters. Patterns varying from 5×5 μm^2 to 50×50 μm^2 were made. Each pattern was generated by alternately scanning the feature at two scan angles (0˚ and 90˚). The number of passes the tip makes over the feature was varied to produce patterns with complete removal of nanoparticles. In this work, a single "pass" is assumed to be scanning from top to bottom (or bottom to top) at a 0˚scan angle or left to right (or right to left) at a 90˚scan angle. One individual image over the feature is considered a single pass, regardless of direction.

To compare commercially available $BaCO_3$ or $CaCO_3$ powder and inhouse prepared nanoparticles, both types were deposited separately on glass substrates to prepare resist films. The suspensions were prepared by dissolving 0.10 g of each compound in 5.0 mL of deionized water. 50 µL aliquots of each suspension were deposited on glass substrates and allowed to dry under ambient conditions for 2 h. Both films were patterned under similar patterning conditions with Tap300DLC probes to observe any differences in the patterning using the two types of nanoparticles. Optical microscope images were compared of both types of resist films.

Gold Evaporation

Gold evaporation was carried out using a diffusion pumped, Edwards AUTO 306 vacuum evaporator at a chamber pressure below 5.0×10^{-6} torr with the substrate heated to 150-220 ˚C using a quartz lamp heater in the evaporation chamber. The gold deposition rate was maintained at approximately 2-3 Å/s and monitored with a quartz crystal microbalance (QCM). Gold films with thicknesses of 40-60 nm were deposited onto substrates. After evaporation, the samples were further annealed at the evaporation temperature for 1 h to ensure better adhesion of the gold to the substrate, and to minimize the surface roughness of the deposited gold micropatterns.[76-78]

Removing Nanoparticle Resist

Conditions for the removal of the salt films were optimized by using various solution-based methods to remove the $CaCO_3$ from the surface. The removal was confirmed by optical and AFM imaging. While both EDTA and HCl were effective at removing the $CaCO_3$ films, the best results were found using a combination of the two solutions. Ca^{2+} is strongly chelated by EDTA.[79-80] Furthermore, most metal carbonates, including $CaCO_3$, react with dilute HCl to produce soluble chlorides, CO_2, and H_2O. These properties have been used to lift the nanoparticle mask once the metal deposition is done on the surface, without damaging the evaporated metal pattern on the surface while completely removing resist material from the surface. Optimization of the resist removal is discussed in a later section. The $CaCO_3$ nanoparticle resist film was removed by sequential soaking of the samples for 2-3 min 10% (w/w) EDTA (aq) at pH 10, followed by 1.0 M HCl (aq). Ultimately, if metal deposited samples were found to have residual salt after this procedure, the gold-patterned samples were sonicated for a few seconds in 10% EDTA (aq) at pH 10 to remove the residual film and excess metal on top of the resist film.

Microplatform characterization

Preliminary characterization of the metal microplatforms was carried out using a Sony Towada XC-999 optical microscope mounted to an AFM. Images were captured using a GrabBee USB 2.0 Video Grabber capture cable and the GrabBee 2.0 software package. Surface topography images were taken with a multimode Nanoscope IIIA scanning probe microscope (Digital Instruments, CA) employing a JV scanner with $110 \times 110\ \mu m^2$ scan range. Non-conductive silicon nitride cantilevers (k ~ 0.12 to 0.06 N/m, NPS from Bruker; Camarillo, CA) were used for all contact mode images. Static plowing of the $CaCO_3$ nanoparticle films and tapping mode images

were carried out using Tap300DLC probes (Budget Sensors k ~ 40 N/m and f ~ 300 kHz). AFM images were analyzed using NanoScope Analysis v1.5 by Bruker Corporation (Camarillo, CA).

Results and Discussion

The development of substrate-tolerant methods for precise fabrication of metal micro- and nano- structures has broad utility for applications including energy harvesting and storage,[8,9-12] biosensing,[2] as well as photonic and plasmonic materials.[3-6] Here, the development of novel salt-based resist films is explored to ultimately increase the versatility of fabrication of such metal structures. The combination of the $CaCO_3$ nanoparticle (NP) resist films with AFM-based patterning and thermal evaporation of the metal allows for the fabrication of metal structures with defined size, shape, and position with a range of different substrates. In addition, the resist removal is straightforward and does not require harsh reagents that could damage the metal structures. The complete fabrication process is outlined in Figure 1. Briefly, the clean substrate is coated with the $CaCO_3$ NP resist layer and patterned using an AFM probe. The patterned substrate is then coated with metal by thermal evaporation. Finally, the $CaCO_3$ NP resist layer, and any excess metal deposited on top of the resist, were removed resulting in an isolated metal microstructure on the substrate. In the following sections, the suitability of various sparingly soluble salts, the resist film deposition conditions, the AFM patterning parameters, and the ability to pattern on a variety of substrates are investigated.

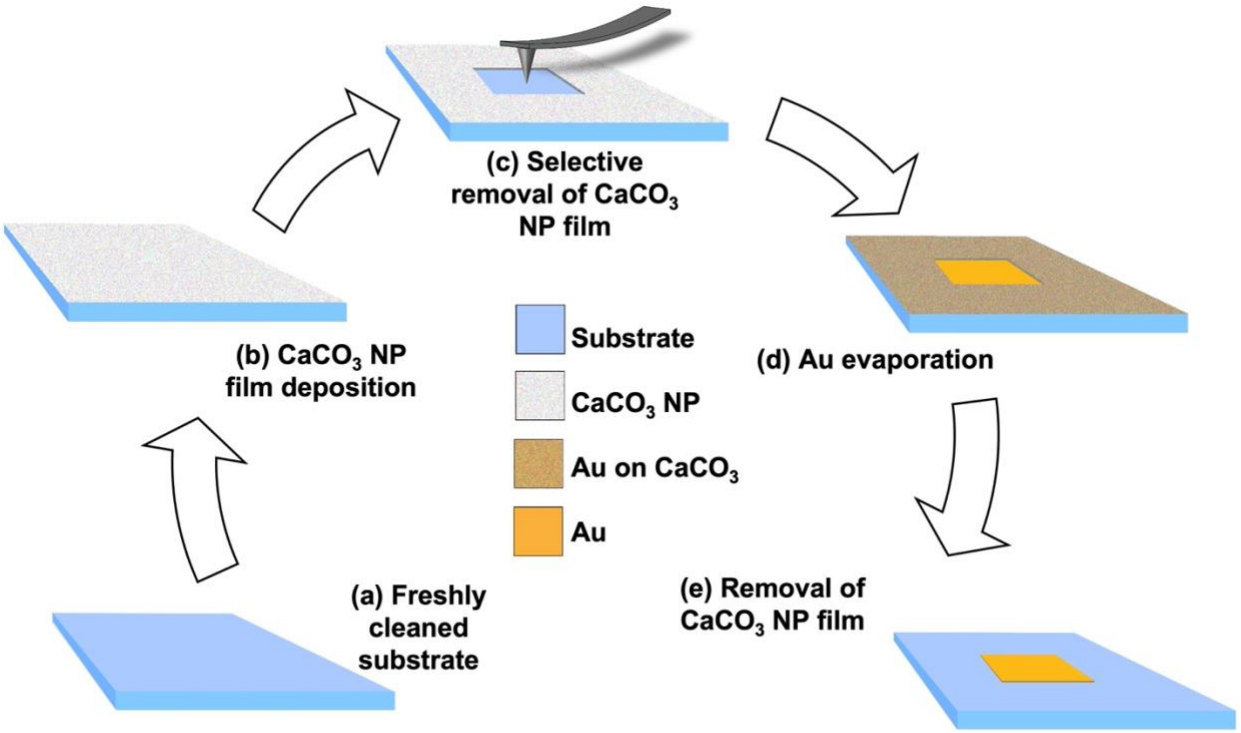

Figure 1: *Schematic diagram of metal microstructure formation on surfaces. (a) Substrate is cleaned and dried. (b) The $CaCO_3$ nanoparticle (NP) suspension is deposited onto the substrate and dried to form a film. (c) A pattern is created using the AFM probe tip to selectively remove an area of the $CaCO_3$ nanoparticle resist film. (d) Gold is evaporated over the entire surface. (e) The $CaCO_3$ nanoparticle resist, and excess metal on top of the resist, are removed while the metallic pattern remains intact on patterned parts of the surface.*

Candidates for Salt-Based Resist Layers

In an attempt to identify a resist material that would be easily patterned and removed from the surface, we explored several different salts including NaCl, $BaCO_3$, and $CaCO_3$ with $CaCO_3$ ultimately being selected. This section briefly discusses the rationale for this choice. NaCl has the advantage that it has good water solubility and would therefore be very easy to remove after the patterning. However, this high solubility made it difficult to create a uniform, thin NaCl film on the substrates. Images of the NaCl films on Si(111) resulting from evaporation of deposited NaCl (aq) solutions, as well as vapor deposition from hot aqueous solution, are shown in supporting information. As shown in Figure S1, macroscopic, uneven, coffee ring structures formed locally

on the surface leaving the remainder of the Si(111) clean when using the solution deposition method. Vapor deposition for 30-45 min proved to be a method that deposited NaCl nanoparticles over wide areas of the surface that could be imaged with AFM, as shown in Figure S2. While we were not able to identify conditions where we could achieve uniform thin films of NaCl nanoparticles, we were able to manipulate the NaCl nanoparticles with an AFM tip to create recognizable patterns on the surface (Figure S3). Such patterned samples were able to withstand thermal evaporation of gold metal onto to the surface, as shown in Figure S4. Soaking the gold-coated, patterned samples in deionized water resulted in incomplete removal of the salt resist and the excess metal deposited on top of the NaCl nanoparticles. Because NaCl did not cover the entire surface, some of the smaller NaCl nanoparticles were fully encased in gold and were not able to be removed in water. These vapor deposited NaCl nanoparticles could not function as true resist layers because of their incomplete surface coverage. It is possible that other deposition processes such as thermal evaporation of the NaCl could be used to deposit uniform layers on samples[81] but this would require further development.

Because of the difficulties associated with uniform deposition of the highly water-soluble NaCl, we explored the deposition of $BaCO_3$ and $CaCO_3$ films. These materials are relatively insoluble in neutral aqueous solution but can be removed by chelation or alteration of the pH. Examples of patterns made on glass using $BaCO_3$ and $CaCO_3$ nanoparticles are presented in Figure 2. We demonstrated that is possible to make patterns in $BaCO_3$ resist films, but we did have difficulty with consistent, clean patterning fabrication, perhaps due to the size of particles or thickness of the films. The features in the $CaCO_3$ are able to be fabricated with cleaner edges and with smaller sizes than the $BaCO_3$. Because of this, and the slightly toxic nature of $BaCO_3$ (compared to $CaCO_3$) and difficulties associated with the synthesis to produce uniform, small

$BaCO_3$ nanoparticles, our focus ultimately became the cleaner alternative, $CaCO_3$. Furthermore, we were able to generate uniform films of $CaCO_3$ and demonstrate that this material was uniformly removed by the AFM patterning process. Therefore, $CaCO_3$ was used for the rest of these investigations.

Salt Nanoparticle Resist Film Structure

$CaCO_3$ nanoparticles were prepared by mixing $Ca(NO_3)_2$ (aq) with $NaNO_3$ (aq) and Na_2CO_3 (aq) in the presence of a surfactant at elevated pH.[72-75] Surfactants aid in obtaining smaller particles with narrower size distribution.[75] Capping the nanoparticles with surfactants may also help reduce the interactions with hydrophilic surfaces, which the particles were deposited onto, and also aids in minimizing aggregation of the particles in solution. As a result, moving the particles with the AFM tip became easier when the particles were smaller and capped with surfactant. Moreover, this resulted in cleaner patterns where the evaporated gold adhered more strongly to the exposed substrate. We tested commercially available $BaCO_3$ and $CaCO_3$ powders as well as in house synthesized $BaCO_3$ and $CaCO_3$ particles (with and without a surfactant).

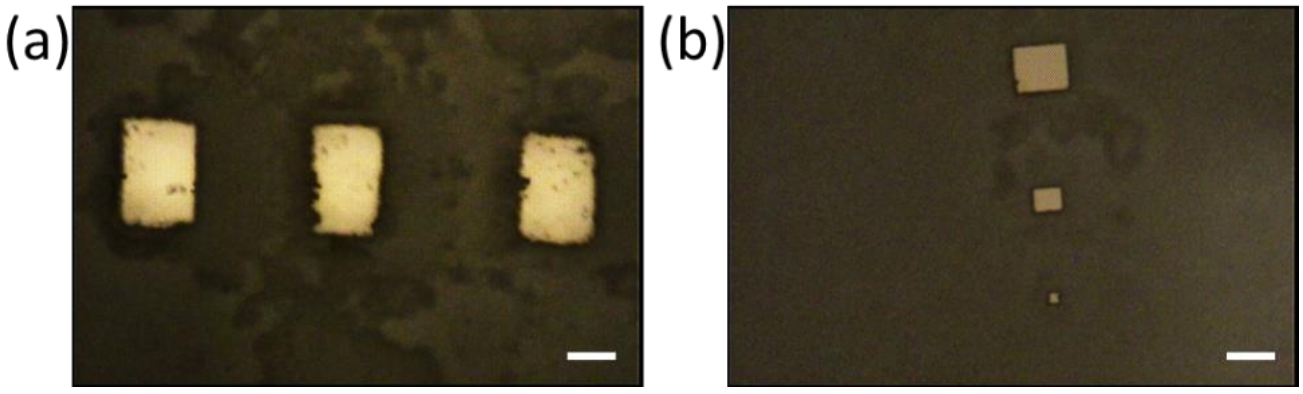

Figure 2: *Optical microscope images on glass substrates of AFM-fabricated patterns in the resist film prepared from (a) commercially available $BaCO_3$ and (b) in house prepared $CaCO_3$ NP capped with triton-x 100. Patterns with brighter contrast (exposed substrate) in a darker background ($BaCO_3$/$CaCO_3$ cover) are presented with a 50 μm scalebar.*

The contrast between patterns on glass substrates made using commercial $BaCO_3$ powder and capped $CaCO_3$ nanoparticles is shown in Figure 2. Patterns made in films of commercial $BaCO_3$ particle films often have less well-defined edges and incomplete patterns due to incomplete removal of the nanoparticles in the patterned area. Uncapped nanoparticles also aggregated in solution, likely due to strong interparticle interactions. In contrast, the in house synthesized, surfactant-capped nanoparticles made uniform films that were easier to pattern, resulting in sharper, more well-defined features. Dynamic light scattering measurements were carried out in triplicate on the nanoparticle solutions using a NanoBrook Omni and showed that in house synthesized $CaCO_3$ particles had a smaller mean radius (580 ± 50 nm) compared to both the commercially available $CaCO_3$ (1520 ± 30 nm) and $BaCO_3$ (830 ± 70 nm) powders. The Tap300DLC AFM probes used in this work typically have a tip radius less than 15 nm, which is much smaller than the nanoparticle diameter. Therefore, the resolution of this technique likely depends on the size of the nanoparticles used in the resist film, rather than the radius of the AFM tip, used to create the patterns.

Surface coverage optimization

An optimal nanoparticle resist film should be thick enough to cover the substrate well, while remaining thin enough to be removed with an AFM tip. Therefore, the nanoparticle film should be thinner than the height of the probe used for patterning. The Tap300DLC AFM probes have an average tip height of 15 μm. The thickness and patternability of the $CaCO_3$ nanoparticle film were optimized by controlling the amount of nanoparticles deposited onto each surface, as shown in Table 1. The amount of nanoparticles was controlled by varying the suspension's concentration (by dilution) and the volume of solution deposited on the substrate. The "relative amount deposited" is a unitless quantity to compare the amount deposited relative to that

when 50 μL of the 0.10 g/5.00 mL stock solution of $CaCO_3$ particles was used (this is normalized to a relative concentration of 1.0). Other amounts are relative to this amount (*e.g.,* using the same 50 μL, but with a 1:1 dilution of the stock solution with buffer decreases the amount deposited by a factor of two, resulting in a relative amount deposited of 0.5) The original $CaCO_3$ nanoparticle stock solution was prepared by suspending 0.1 g of the in-house synthesized $CaCO_3$ nanoparticles in 5 mL of deionized water. Clean glass substrates with a surface area of approximately 1 cm^2 were prepared with 50 μL and 100 μL aliquots of nanoparticle suspensions with different dilutions. Patterns were made using AFM and the surfaces were characterized using optical microscopy. The "Number of Passes" describes how many AFM scans were made over an area before a clear pattern was observed under the optical microscope as defined in the materials and methods section. Figure 3 shows that the number of imaging passes required for patterning increases with the relative amount of $CaCO_3$ deposited on the surface.

Table 1: *Optimization of $CaCO_3$ coverage.*

	DILUTION FACTOR ($V_{salt\ soln}$:V_{H_2O})	**VOLUME ADDED (μL)**	**RELATIVE AMOUNT DEPOSITED**
A*	**1:0**	**50**	**1.00**
B*	**1:1**	**50**	**0.500**
C1	**1:3**	**50**	**0.250**
C2*	**1:3**	**100**	**0.500**
D1	**1:5**	**50**	**0.167**
D2	**1:5**	**100**	**0.333**
E1	**1:7**	**50**	**0.125**
E2	**1:7**	**100**	**0.250**

F**	**1:9**	**50**	**0.100**

*Unable to be patterned
** Incomplete coverage of resist film

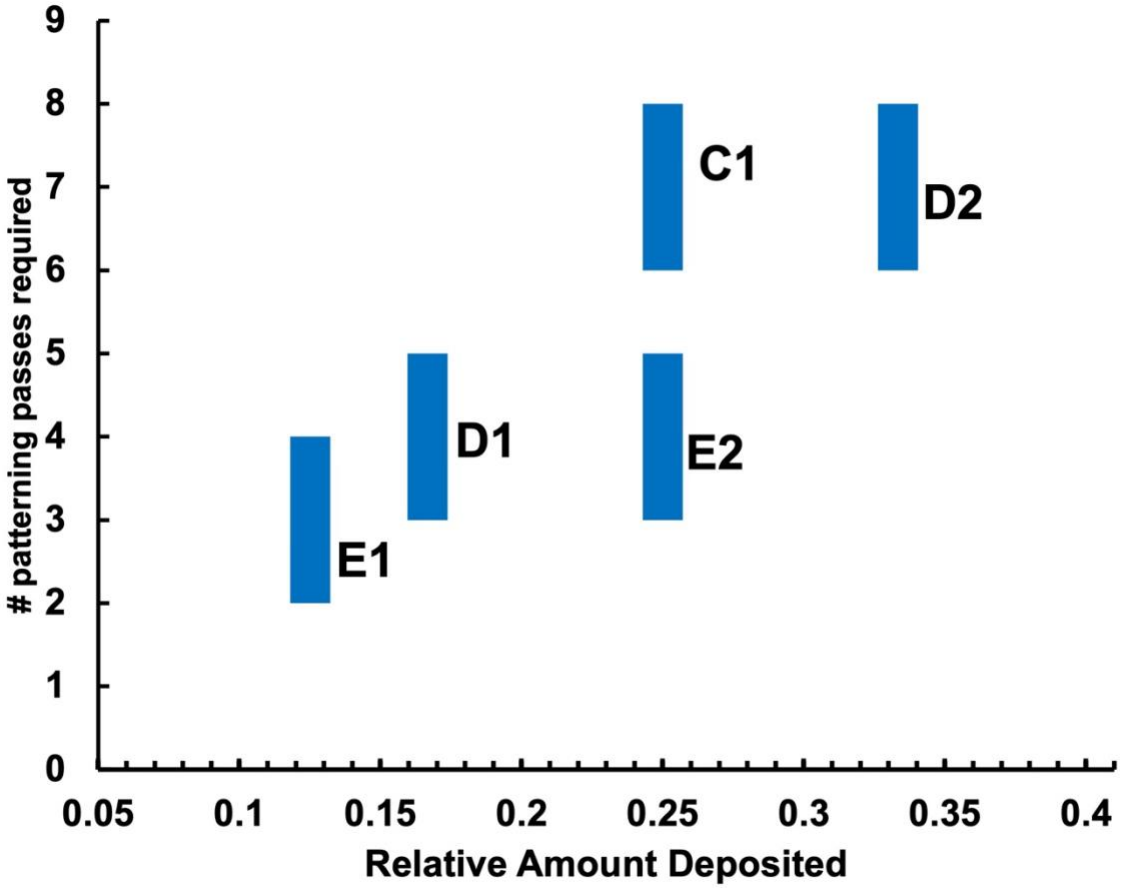

Figure 3: The number of AFM patterning passes required as a function of relative amount of $CaCO_3$ added to the surface. Data points correspond to entries in Table 1. Height of the bars represents the variation in the required number of passes observed. Several of the experiments are not included, due to the inability to pattern the film (A, B, C2) or incomplete film formation (F).

The original, undiluted nanoparticle suspension and 1:1 dilution (conditions A and B of *Table 1*) were too concentrated and yielded a thick nanoparticle film on the surface. An AFM tip was unable to pattern these films, likely because the nanoparticle film thickness exceeded the height of the probe. Solutions C through E provided a uniform surface coverage, yet were patternable with a reasonable number of AFM scans. The required number of passes went down,

as expected, as the nanoparticle solution was systematically diluted and the relative amount of nanoparticles deposited decreased (Figure 3). A 1:9 dilution (Solution F) resulted in an incomplete nanoparticle coverage on the surface as observed by an optical microscope, and so was unsuitable for use as a resist film.

Effect of patterning parameters

Figure 4 illustrates the process for investigating effects of patterning parameters. While many of the scanning parameters are not critical for removal of the nanoparticle films, the tip velocity and applied force have large effects on the patterning process. The optimal parameters will vary depending on the thickness and density of the nanoparticle film, therefore all trials were performed using conditions described in section D1 of Table 1 on 1×1 cm^2 glass substrates.

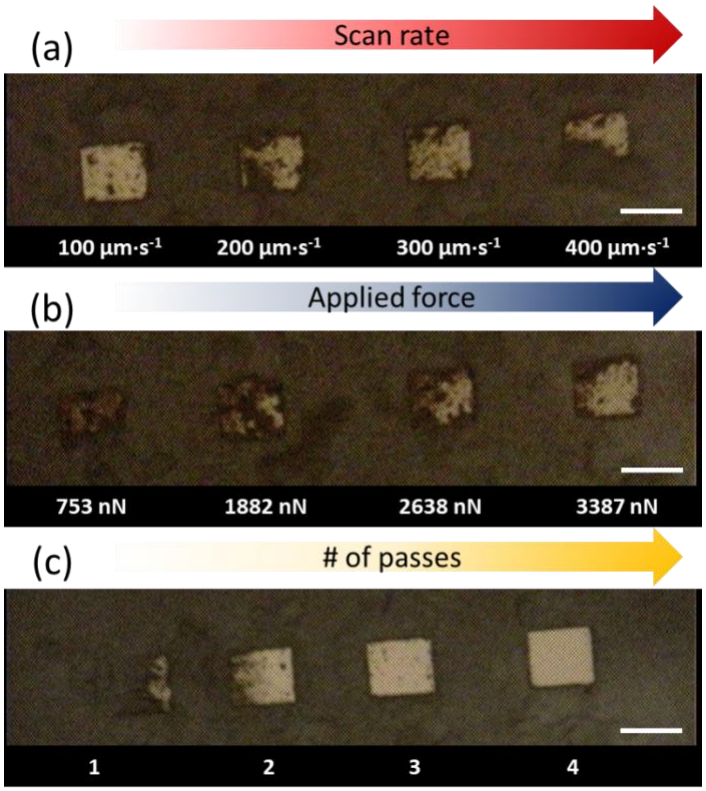

Figure 4*: Optical images showing the variation in patterning integrity with the AFM patterning parameters. Micropattern formation as a function of (a) tip velocity (b) applied force (set point) on AFM probe and (c) number of scans. All studies were conducted on nanoparticle resist films made utilizing NP solution conditions Table 1 D1. All patterns were 50×50 µm^2. Tip velocity (a) was tested at a force of ~3500 nN by scanning over the surface once. Effects of applied force (b) was tested at constant tip velocity of 300 µm·s^{-1} by scanning over the surface once. Number of scans was tested while setting a force of ~3500 nN at a tip velocity of 300 µm·s^{-1}constant to all samples. All patterns were made on glass substrates and reported images were collected using an optical microscope after the patterning experiments without gold evaporation with a 50 µm scalebar. Dark color in the images is the nanoparticle cover while patterned areas are bright due to the reflectivity of the exposed glass surface.*

Patterns in Figure 4a have been made utilizing 100, 200, 300, and 400 µm·s^{-1} tip velocity, respectively. These images indicate that the smaller tip velocities remove nanoparticle resists better than faster scan rates. Although faster tip velocities produce higher momentum, it may also result in the AFM tip not tracking the surface well. Another possibility is that the cantilever can twist at faster tip velocities limiting its ability to fully transfer its momentum to the nanoparticle resist

layer. Earlier work from several groups laid the foundation to investigate the effect of patterning parameters on molecular level resist films,[61-62, 82] and our observations are in good agreement with these reports. The amount of nanoparticles cleared from an area increased as the applied load on surface increased (Figure 4b). As the applied load increased, the tip's ability to penetrate the nanoparticle film and consistently remove the nanoparticles from the surface during imaging increased. The number of passes required to form a clean pattern is shown in Figure 4c, while maintaining a ~3500 nN force at a scan rate of 300 $\mu m \cdot s^{-1}$. Scans were made at angles of 0˚ and 90˚, alternatively, to ensure even edges on all four sides of the patterned feature. The first two patterns in Figure 4c were made with one and two passes, respectively. With fewer passes, the $CaCO_3$ nanoparticles are not completely removed, leading to incomplete pattern formation. Three passes resulted in patterns with resolved edges, but some residual nanoparticles are still left in the patterned area (Figure 4c). Patterns with residual nanoparticles result in rough, poor-adhering gold features that can partially peel off the substrate during resist film removal. Four passes completely removed all traces of nanoparticles, resulting in a fully cleared area. Based on the conditions studied, the nanoparticle resist film patterning can be done by using a range of conditions. We were able to achieve clean patterns by using tip velocities ranging from 200 to 300 $\mu m \cdot s^{-1}$ and applied forces between 2500-3500 nN. The AFM probe tip was moved over a desired area 4-6 times, alternating between 0˚and 90˚scan angles.

Substrate and Size Dependence of Patterning

Patterning of the nanoparticle resist was achieved by passing a stiff AFM probe tip across the thin nanoparticle film on the desired substrate. We investigated 1) the adaptability towards different substrates commonly used in surface chemistry applications and 2) ability and limitations of the technique towards producing large and small structures. We chose glass, silicon, and mica

surfaces given their ubiquity in applications including biosensor development, biocompatibility, lab on a chip device, and photovoltaic devices and widespread use in previous fabrication processes. Furthermore, all these substrates can be easily cleaned using established methods and can be subjected to thermal evaporation or sputter-coating. Using a large scanner with ~110×110 μm^2 range, we produced patterns as large as 80×80 μm^2. The smallest patterns that were attempted were 2×2 μm^2. Patterns above 5×5 μm^2 were visible through the optical microscope mounted to the AFM. The tip velocity was maintained by increasing the scan rate for smaller patterns, therefore smaller patterns can be made significantly faster than larger patterns. The relative location of the different features on the substrate was controlled by changing the X-Y offsets of the microscope scan, or by manually moving the microscope stage.

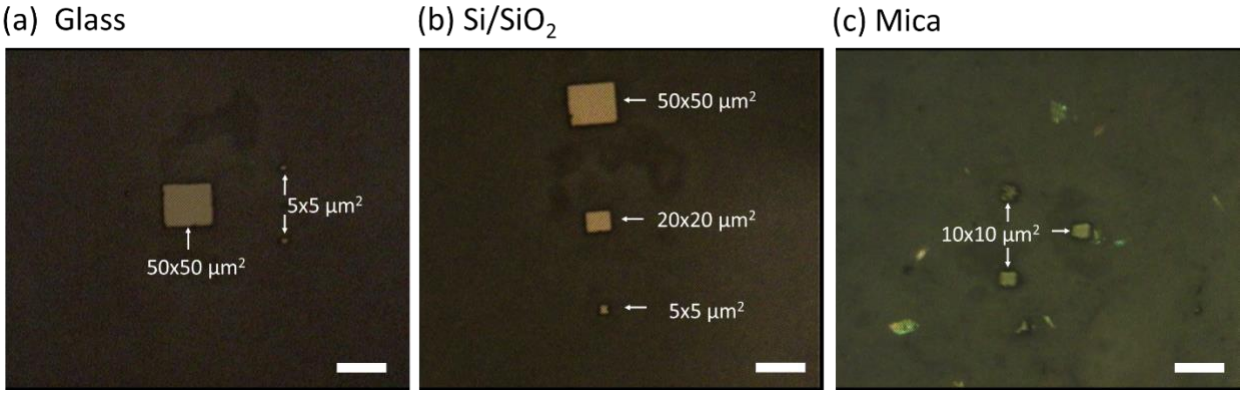

Figure 5: *Optical microscope images of patterns in nanoparticle resist films on (a) glass, (b) silicon, and (c) mica substrates with 50 µm scalebars. Dark areas represent the nanoparticle resist film while bright square shapes indicate patterned locations of different sizes where the underlying substrate has been exposed, before the gold evaporation. Patterns were made using a tip velocity of 200 $\mu m \cdot s^{-1}$ and a setpoint of ~3500 nN. The AFM probe tip was moved over a desired area 6 times, alternating between 0˚ and 90˚ scan angles as described earlier.*

Figure 5 demonstrates patterns of a range of sizes made on glass (a), silicon (b), and mica (c) substrates. The ease of plowing the resist film was not found to be substrate dependent. Optical microscope images showed different contrast for different substrates, due to differences

in reflectivity of the different substrates, but bright spots on the surfaces are always areas where the $CaCO_3$ nanoparticle resist had been patterned, exposing the underlying substrate. Not only were we able to pattern on a variety of substrates, the patterns appear durable and can be observed from days to months later. While typical processing and handling of the substrates once patterned did not result in compromise of the integrity of the patterns, occasionally some particles were observed to move into the patterned areas.

To explore the flexibility of this patterning approach, other methods for selective removal of the nanoparticles in addition to the AFM -based methods were explored. For example, a number of micro milling tools and techniques have been developed over the years with different plowing properties which show potential to be modified to pattern similarly[83]. We have used diamond or tungsten carbide scribes to manually remove the nanoparticle resist film once the surface is prepared, with clean boundaries (Figure S5). Use of such tools to make larger scale patterns broadens the applicability of the method but will not be suitable for nano-sized patterns.

Gold evaporation

Gold was evaporated onto patterned substrates in a metal evaporator at high vacuum. The chamber was heated during and after the evaporation to ensure a good adhesion of metallic patterns onto the exposed areas of the substrates. Since the nanoparticle resist is physisorbed on surfaces, it can be easily disturbed by an AFM tip, which is an ideal characteristic for patterning purposes. Consequently, even imaging these patterns with tapping mode AFM is challenging because even imaging can move the $CaCO_3$ nanoparticles. Therefore, only optical images of the salt patterns have been shown of these $CaCO_3$ patterns. However, the nanoparticle resist becomes more stable after evaporating gold onto the sample. Therefore, measuring the thickness of the nanoparticle resist was done using tapping mode AFM after the gold evaporation. The gold film adds a small

thickness uniformly over the substrate, therefore the cross-sectional heights measured of the nanoparticle films should not be affected by the gold layer over it. Figure 6 shows cross-sectional heights of nanoparticle resist films as a function of dilution discussed in Table 1. These cross-sections are imaged across the boundary between the pattern and the salt resist.

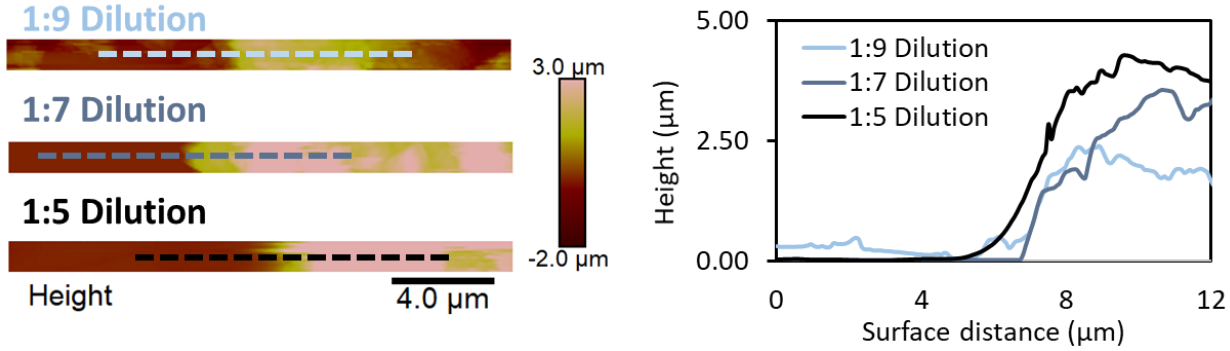

Figure 6: *Cross sections of nanoparticle pattern boundaries as a function of dilution of nanoparticle stock solution. AFM images of cross sections from three different dilutions (Table 1 D1, E1, F) are shown on the right after they had been coated with 50 nm of gold with their cross sections along the respective dotted lines on the AFM images on the left.*

The height profiles of nanoparticle thin films were measured to have thicknesses around ~ 2 µm, ~2.7 µm, and ~3.5 µm respectively at 1:9, 1:7, and 1:5 dilutions. Cross sections for surfaces with larger amounts of nanoparticles (more concentrated solutions) resulted in films thicker than the Z scan range of the microscope and therefore were unable to be measured. These post-evaporation profiles demonstrate the persistence of the patterns after the gold evaporation process. However, to complete the process, the resist film must be removed along with the lift-off of the gold outside the patterns. This is discussed in the next section.

Nanoparticle resist removal

In this work, we investigated two possible ways to remove the nanoparticle resist layer as described earlier: (1) by using reactivity of group IIA carbonates with dilute HCl, and (2) utilizing the chelating ability of EDTA towards Ca^{2+} ions.[79-80] Although both methods were successful for

removing nanoparticle films, EDTA removal was chosen to dissolve the nanoparticle resist after gold deposition. The reaction of metal cations with EDTA is mild and slow, while acid dissolution produced CO_2 bubbles that occasionally delaminated some of the gold patterns. This is therefore our chosen first step for resist removal. However, residual particles sometimes remained on the surface following the initial EDTA treatment. In such cases, the residual particles were subsequently removed using a brief (few seconds) dissolution in dilute HCl. In rare cases where some residual particles remained after these two steps, a brief sonication in basic 10% EDTA was also used to ensure surfaces were free from nanoparticles. Generally, gold shows stronger adhesion to mica substrates, while glass and silica surfaces often require an adhesion layer of Cr or Ti to bridge the mismatch between the surface energies of Au and SiO_2.[84] In this work, we have not used an adhesion layer on any of the substrates and the resulting metallic microfeatures withstood short sonication times. This indicates that the gold patterns adhere reasonably well on substrates tested. Some smaller features ($< 5\ \mu m^2$) were often removed in the resist removal process, indicating possible weak adhesion. The inclusion of evaporation of an adhesion layer before the gold evaporation could be used to increase the adhesion, but this has not been explored here.

Gold Micropattern Characterization

Once the nanoparticle resist was removed, the gold micropatterns were characterized using optical microscopy and AFM imaging. Optical microscope images (Figure 7a) clearly showed nearly the entire resist film, and excess gold metal deposited on top of the resist film, were removed upon EDTA, HCl, and sonication treatment. AFM images (Figure 7b) further confirmed that the surface was mostly free from the nanoparticle resist. Isolated nanoparticle clusters were seen in some of the AFM images, but these imperfections were too small to be seen under the optical microscope images. AFM images further revealed that the patterns are smooth and uniform across

the surface, with some small pinholes in the gold features, possibly resulting from residual nanoparticles in the patterning area. The features' edges were defined in most cases. However, there were places with poor definition, especially when the pattern dimensions were 5 µm or less.

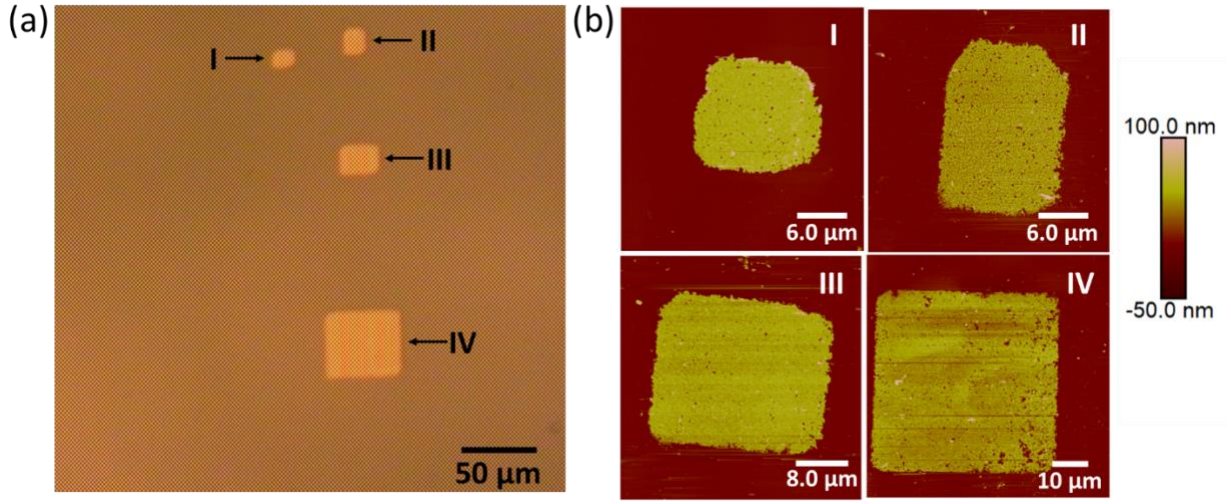

Figure 7: *Optical microscope (a) and AFM images (b) of micropatterns made on a glass substrate after gold evaporation and resist removal with respective scalebars. Four features (I) 10×10 µm², (II) 10×15 µm², (III) 20×30 µm², and (IV) 50×50 µm² respectively are shown with their AFM images.*

Patterns smaller than 5×5 µm² often peeled off during the nanoparticle removal process. This is likely due to the smaller contact area of these patterns with the substrate, resulting weaker adhesion with the surface. To protect these small metal features, the nanoparticle removal process was conducted without sonication. However, this occasionally left residual nanoparticle resist film on the surface. Patterns larger than 20×20 µm² were developed with better edge resolution and definition (Figure 7). Cross sections of the gold platforms (Figure S6) measure heights between 40 – 60 nm, consistent with the expected deposition thicknesses. Furthermore, we successfully demonstrated deposition of gold on micropatterns made on glass, SiO_2 and mica substrates (Figure 8), using discussed patterning, evaporating, and nanoparticle removal methodologies.

The ultimate resolution in terms of size of features that can be fabricated using this method has not been explored in this work. Features smaller than 5×5 µm² were more difficult to fabricate,

and did not appear to adhere well to some substrates. This could be addressed through the incorporation of an adhesion layer in the fabrication process. This might allow even smaller features to remain on the surface. However, this technique will not likely be able to fabricate features smaller than the particle size used in the resist layer. In these initial experiments, it is clear that the particle size was relatively large (see Salt Resist Film Structure Section). This will likely provide a lower limit to the size of features that can be fabricated (unlike other AFM-based lithography methods which are tip limited). It is possible that much smaller $CaCO_3$ particles could be fabricated and used as resists, and this should allow the fabrication of nanoscale features if the adhesion is addressed.

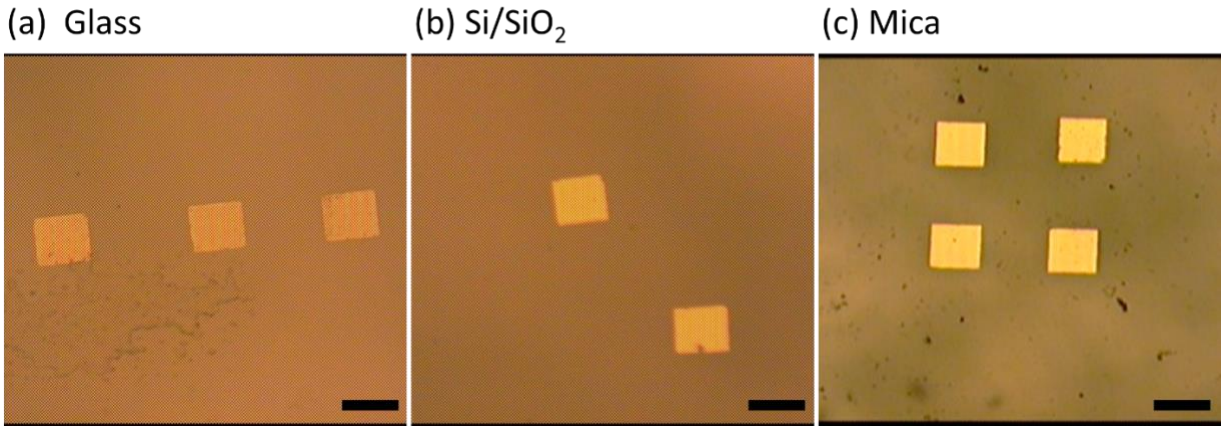

Figure 8: *Optical microscope images of gold micropatterns made on (a) glass, (b) silicon, and (c) mica surfaces once the nanoparticle resist is completely removed with scalebars of 50 µm. Minimum traces of the nanoparticle resist are observed while defined gold features are intact to the surface.*

Conclusions

Here, a method for metal microstructure fabrication has been demonstrated in which a thin layer of salt acts as a versatile, robust resist layer that can withstand deposition conditions unsuitable for other commonly used organic resist materials on a variety of substrates. In this work we demonstrated the use of AFM to pattern a salt-based, nanoparticle film that serves as a resist

layer in order to expose an underlying substrate, and thereby evaporate metal through the patterns to fabricate metallic microstructures. In this pilot study, we have synthesized $CaCO_3$ nanoparticles and formed uniform thin films of nanoparticles on different surfaces. Nanoparticle coverage and patterning parameters were optimized to selectively remove nanoparticles from the surface to expose the underlying substrate. Patterns with sharp edges were created using tip velocities ranging from 200-300 $\mu m \cdot s^{-1}$ and forces between 2500-3500 nN by patterning over the nanoparticle resist 4-6 times at alternating scan directions (0˚ and 90˚). Once gold was evaporated, and the nanoparticle film as well as excess metal were removed from the substrate surface, fabricated metal features were imaged using optical microscopy and AFM. Features under 5×5 to 80×80 μm^2 were successfully fabricated. Furthermore, metal evaporation can potentially be replaced by sputter coating, allowing for further flexibility in metals that can be successfully fabricated. Although smaller patterns could be more useful for nanoscale applications, such patterns showed poor adhesion on to the glass and mica substrates tested but could potentially be improved by using an adhesive layer of precursor metal to bridge the surface energy gap. This method of microstructure fabrication with precise spatial registry and is expected to find utility in applications including biosensing, photonic and plasmonic structures, and electronics.

Supporting Information

A description of the procedure for NaCl and $BaCO_3$ resist film formation and fabrication, optical and AFM images of NaCl resist films along with patterns created in the NaCl resists. Particle size distributions for the NaCl, optical images of patterns made in $CaCO_3$ with scribes, and AFM images and cross-sections of gold patterns created on glass are provided in the SI.

Acknowledgements

This work was supported in part by the National Science Foundation under Grant CHE-2108448 as well as a Strategic Initiative Grant from the University of Kansas. The DLS data were collected in the TORP Laboratory at the University of Kansas.

References

1. Wang, Y.; Mirkin, C. A.; Park, S.-J. Nanofabrication Beyond Electronics. *ACS Nano* **2009,** *3*, 1049-1056.

2. Anker, J. N.; Hall, W. P.; Lyandres, O.; Shah, N. C.; Zhao, J.; Van Duyne, R. P. Biosensing with Plasmonic Nanosensors. *Nat. Mater.* **2008,** *7*, 442-453.

3. Near, R.; Tabor, C.; Duan, J.; Pachter, R.; El-Sayed, M. Pronounced Effects of Anisotropy on Plasmonic Properties of Nanorings Fabricated by Electron Beam Lithography. *Nano Lett.* **2012,** *12*, 2158-2164.

4. Päivänranta, B.; Merbold, H.; Giannini, R.; Büchi, L.; Gorelick, S.; David, C.; Löffler, J. F.; Feurer, T.; Ekinci, Y. High Aspect Ratio Plasmonic Nanostructures for Sensing Applications. *ACS Nano* **2011,** *5*, 6374-6382.

5. Chong, X.; Zhang, Y.; Li, E.; Kim, K.-J.; Ohodnicki, P. R.; Chang, C.-h.; Wang, A. X. Surface-Enhanced Infrared Absorption: Pushing the Frontier for On-Chip Gas Sensing. *ACS Sensors* **2018,** *3*, 230-238.

6. Deng, W.; Goldys, E. M. Plasmonic Approach to Enhanced Fluorescence for Applications in Biotechnology and the Life Sciences. *Langmuir* **2012,** *28*, 10152-10163.

7. Khlebtsov, B. N.; Khanadeev, V. A.; Burov, A. M.; Le Ru, E. C.; Khlebtsov, N. G. Reexamination of Surface-Enhanced Raman Scattering from Gold Nanorods as a Function of Aspect Ratio and Shape. *J. Phys. Chem. C* **2020,** *124*, 10647-10658.

8. Huang, Q.; Shen, W.; Fang, X.; Chen, G.; Yang, Y.; Huang, J.; Tan, R.; Song, W. Highly Thermostable, Flexible, Transparent, and Conductive Films on Polyimide Substrate with an AZO/AgNW/AZO Structure. *ACS Appl. Mater. Interfaces* **2015,** *7*, 4299-4305.

9. Furube, A.; Hashimoto, S. Insight into Plasmonic Hot-Electron Transfer and Plasmon Molecular Drive: New Dimensions in Energy Conversion and Nanofabrication. *NPG Asia Mater.* **2017,** *9*, e454-e454.

10. Hildebrandt, N.; Spillmann, C. M.; Algar, W. R.; Pons, T.; Stewart, M. H.; Oh, E.; Susumu, K.; Díaz, S. A.; Delehanty, J. B.; Medintz, I. L. Energy Transfer with Semiconductor Quantum Dot Bioconjugates: A Versatile Platform for Biosensing, Energy Harvesting, and Other Developing Applications. *Chem. Rev. (Washington, DC, U. S.)* **2017,** *117*, 536-711.

11. Robel, I.; Subramanian, V.; Kuno, M.; Kamat, P. V. Quantum Dot Solar Cells. Harvesting Light Energy with CdSe Nanocrystals Molecularly Linked to Mesoscopic TiO_2 Films. *J. Am. Chem. Soc.* **2006,** *128*, 2385-2393.

12. Scott, R.; Kirkeminde, A.; Gong, M.; Totleben, J.; Ren, S.; Tuinenga, C.; Lewis, C.; Luo, H.; Higgins, D.; Chikan, V. Impact of Indiumand Gallium Doping on the Photovoltaic Performance of CdSe Quantum Dot Hybrid Solar Cells. *ECS Trans.* **2015,** *66*, 1-8.

13. Alamri, M.; Liu, B.; Sadeghi, S. M.; Ewing, D.; Wilson, A.; Doolin, J. L.; Berrie, C. L.; Wu, J. Graphene/WS_2 Nanodisk Van der Waals Heterostructures on Plasmonic Ag Nanoparticle-Embedded Silica Metafilms for High-Performance Photodetectors. *ACS Appl. Nano Mater.* **2020,** *3*, 7858-7868.

14. Christopher, P.; Xin, H.; Marimuthu, A.; Linic, S. Singular Characteristics and Unique Chemical Bond Activation Mechanisms of Photocatalytic Reactions on Plasmonic Nanostructures. *Nat. Mater.* **2012,** *11*, 1044-1050.

15. Cao, Y.; Yang, Y.; Shan, Y.; Huang, Z. One-Pot and Facile Fabrication of Hierarchical Branched Pt–Cu Nanoparticles as Excellent Electrocatalysts for Direct Methanol Fuel Cells. *ACS Appl. Mater. Interfaces* **2016,** *8*, 5998-6003.

16. Bai, F.; Sun, Z.; Wu, H.; Haddad, R. E.; Xiao, X.; Fan, H. Templated Photocatalytic Synthesis of Well-Defined Platinum Hollow Nanostructures with Enhanced Catalytic Performance for Methanol Oxidation. *Nano Lett.* **2011,** *11*, 3759-3762.

17. Hong, C.; Jin, X.; Totleben, J.; Lohrman, J.; Harak, E.; Subramaniam, B.; Chaudhari, R. V.; Ren, S. Graphene Oxide Stabilized Cu_2O for Shape Selective Nanocatalysis. *J. Mater. Chem. A* **2014,** *2*, 7147-7151.

18. Requejo, K. I.; Liopo, A. V.; Derry, P. J.; Zubarev, E. R. Accelerating Gold Nanorod Synthesis with Nanomolar Concentrations of Poly(vinylpyrrolidone). *Langmuir* **2017,** *33*, 12681-12688.

19. Roh, J.; Yi, J.; Kim, Y. Rapid, Reversible Preparation of Size-Controllable Silver Nanoplates by Chemical Redox. *Langmuir* **2010,** *26*, 11621-11623.

20. Boulanger, C. Thermoelectric Material Electroplating: A Historical Review. *J. Electron. Mater.* **2010,** *39*, 1818-1827.

21. Sullivan, A. M.; Kohl, P. A. The Autocatalytic Deposition of Gold in Nonalkaline, Gold Thiosulfate Electroless Bath. *J. Electrochem. Soc.* **1995,** *142*, 2250-2255.

22. Osaka, T.; Okinaka, Y.; Sasano, J.; Kato, M. Development of New Electrolytic and Electroless Gold Plating Processes for Electronics Applications. *Sci. Technol. Adv. Mater.* **2006,** *7*, 425-437.

23. Hämäläinen, J.; Ritala, M.; Leskelä, M. Atomic Layer Deposition of Noble Metals and Their Oxides. *Chem. Mater.* **2014,** *26*, 786-801.

24. Dorp, W. F. v.; Hagen, C. W. A Critical Literature Review of Focused Electron Beam Induced Deposition. *J. Appl. Phys.* **2008,** *104*, 081301.

25. Mattox, D. M. Chapter 4 - Physical Sputtering and Sputter Deposition. *The Foundations of Vacuum Coating Technology (Second Edition)*, Mattox, D. M., Ed. William Andrew Publishing: 2018, pp 87-149.

26. Ludwig, C.; Wochele, J.; Jörimann, U. Measuring Evaporation Rates of Metal Compounds from Solid Samples. *Anal. Chem.* **2007,** *79*, 2992-2996.

27. Schwartz, D. K. Mechanisms and Kinetics of Self-Assembled Monolayer Formation. *Annu. Rev. Phys. Chem.* **2001,** *52*, 107-137.

28. Vericat, C.; Vela, M. E.; Benitez, G. A.; Gago, J. A. M.; Torrelles, X.; Salvarezza, R. C. Surface Characterization of Sulfur and Alkanethiol Self-Assembled Monolayers on Au(111). *J. Phys.: Condens. Matter* **2006,** *18*, R867-R900.

29. Vericat, C.; Vela, M. E.; Corthey, G.; Pensa, E.; Cortés, E.; Fonticelli, M. H.; Ibañez, F.; Benitez, G. E.; Carro, P.; Salvarezza, R. C. Self-Assembled Monolayers of Thiolates on Metals: A Review Article on Sulfur-Metal Chemistry and Surface Structures. *RSC Adv.* **2014,** *4*, 27730-27754.

30. Sellers, H.; Ulman, A.; Shnidman, Y.; Eilers, J. E. Structure and Binding of Alkanethiolates on Gold and Silver Surfaces: Implications for Self-Assembled Monolayers. *J. Am. Chem. Soc.* **1993,** *115*, 9389-9401.

31. Tripp, C. P.; Hair, M. L. An Infrared Study of the Reaction of Octadecyltrichlorosilane with Silica. *Langmuir* **1992,** *8*, 1120-1126.

32. Fadeev, A. Y.; McCarthy, T. J. Trialkylsilane Monolayers Covalently Attached to Silicon Surfaces: Wettability Studies Indicating that Molecular Topography Contributes to Contact Angle Hysteresis. *Langmuir* **1999,** *15*, 3759-3766.

33. Aizawa, M.; Buriak, J. M. Block Copolymer-Templated Chemistry on Si, Ge, InP, and GaAs Surfaces. *J. Am. Chem. Soc.* **2005,** *127*, 8932-8933.

34. Aizawa, M.; Buriak, J. M. Block Copolymer Templated Chemistry for the Formation of Metallic Nanoparticle Arrays on Semiconductor Surfaces. *Chem. Mater.* **2007,** *19*, 5090-5101.

35. Porter, L. A.; Ribbe, A. E.; Buriak, J. M. Metallic Nanostructures via Static Plowing Lithography. *Nano Lett.* **2003,** *3*, 1043-1047.

36. D'Acunto, M.; Napolitano, S.; Pingue, P.; Giusti, P.; Rolla, P. Fast Formation of Ripples Induced by AFM. A New Method for Patterning Polymers on Nanoscale. *Mater. Lett.* **2007,** *61*, 3305-3309.

37. Na, J. Y.; Kang, B.; Sin, D. H.; Cho, K.; Park, Y. D. Understanding Solidification of Polythiophene Thin Films during Spin-Coating: Effects of Spin-Coating Time and Processing Additives. *Sci. Rep.* **2015,** *5*, 13288.

38. Apanius, M.; Kaul, P. B.; Abramson, A. R. Silicon Shadow Mask Fabrication for Patterned Metal Deposition with Microscale Dimensions Using a Novel Corner Compensation Scheme. *Sens. Actuators, A* **2007,** *140*, 168-175.

39. Vazquez-Mena, O.; Sannomiya, T.; Villanueva, L. G.; Voros, J.; Brugger, J. Metallic Nanodot Arrays by Stencil Lithography for Plasmonic Biosensing Applications. *ACS Nano* **2011,** *5*, 844-853.

40. Wendeln, C.; Ravoo, B. J. Surface Patterning by Microcontact Chemistry. *Langmuir* **2012,** *28*, 5527-5538.

41. Liu, J.; Xu, G.; Rochford, C.; Lu, R.; Wu, J.; Edwards, C. M.; Berrie, C. L.; Chen, Z.; Maroni, V. A. Doped Graphene Nanohole Arrays for Flexible Transparent Conductors. *Appl. Phys. Lett.* **2011,** *99*, 023111.

42. Lou, Q.; Shipp, D. A. Imprint Lithography with Degradable Elastomeric Polyanhydrides. *ACS Appl. Mater. Interfaces* **2012,** *4*, 4457-4460.

43. Traub, M. C.; Longsine, W.; Truskett, V. N. Advances in Nanoimprint Lithography. *Annu. Rev. Chem. and Biomol. Eng.* **2016,** *7*, 583-604.

44. Gates, B. D.; Xu, Q.; Stewart, M.; Ryan, D.; Willson, C. G.; Whitesides, G. M. New Approaches to Nanofabrication: Molding, Printing, and Other Techniques. *Chem. Rev.* **2005,** *105*, 1171-1196.

45. Nyffenegger, R. M.; Penner, R. M. Nanometer-Scale Surface Modification Using the Scanning Probe Microscope: Progress since 1991. *Chem. Rev.* **1997,** *97*, 1195-1230.

46. Chen, Y. Nanofabrication by Electron Beam Lithography and Its Applications: A Review. *Microelectron. Eng.* **2015,** *135*, 57-72.

47. Biswas, A.; Bayer, I. S.; Biris, A. S.; Wang, T.; Dervishi, E.; Faupel, F. Advances in Top–down and Bottom–Up Surface Nanofabrication: Techniques, Applications & Future Prospects. *Adv. Coll. Interface Sci.* **2012,** *170*, 2-27.

48. Ulapane, S. B.; Kamathewatta, N. J. B.; Borkowski, A. K.; Steuart, S. J.; Berrie, C. L. Periodic Silver and Gold Nanodot Array Fabrication on Nanosphere Lithography-Based Patterns Using Electroless Deposition. *J. Phys. Chem. C* **2020,** *124*, 15646-15655.

49. Brown, K. A.; Hedrick, J. L.; Eichelsdoerfer, D. J.; Mirkin, C. A. Nanocombinatorics with Cantilever-Free Scanning Probe Arrays. *ACS Nano* **2019,** *13*, 8-17.

50. Salaita, K.; Wang, Y.; Mirkin, C. A. Applications of dip-pen nanolithography. *Nat. Nanotechnol.* **2007,** *2*, 145-155.

51. Wu, C.-C.; Reinhoudt, D. N.; Otto, C.; Subramaniam, V.; Velders, A. H. Strategies for Patterning Biomolecules with Dip-Pen Nanolithography. *Small* **2011,** *7*, 989-1002.

52. Bellido, E.; Cardona-Serra, S.; Coronado, E.; Ruiz-Molina, D. Assisted-Assembly of Coordination Materials into Advanced Nanoarchitectures by Dip Pen Nanolithography. *Chem. Comm.* **2011,** *47*, 5175-5177.

53. Basnar, B.; Weizmann, Y.; Cheglakov, Z.; Willner, I. Synthesis of Nanowires Using Dip-Pen Nanolithography and Biocatalytic Inks. *Adv. Mater.* **2006,** *18*, 713-718.

54. Masubuchi, S.; Arai, M.; Machida, T. Atomic Force Microscopy Based Tunable Local Anodic Oxidation of Graphene. *Nano Lett.* **2011,** *11*, 4542-4546.

55. Held, R.; Heinzel, T.; Studerus, P.; Ensslin, K. Nanolithography by Local Anodic Oxidation of Metal Films Using an Atomic Force Microscope. *Phys. E (Amsterdam, Neth.)* **1998,** *2*, 748-752.

56. Kozhukhov, A. S.; Scheglov, D. V.; Fedina, L. I.; Latyshev, A. V. The Initial Stages of Atomic Force Microscope Based Local Anodic Oxidation of Silicon. *AIP Adv.* **2018,** *8*, 025113.

57. Liu, H.; Hoeppener, S.; Schubert, U. S. Reversible Nanopatterning on Polypyrrole Films by Atomic Force Microscope Electrochemical Lithography. *Adv. Funct. Mater.* **2016,** *26*, 614-619.

58. Albisetti, E.; Carroll, K. M.; Lu, X.; Curtis, J. E.; Petti, D.; Bertacco, R.; Riedo, E. Thermochemical Scanning Probe Lithography of Protein Gradients at the Nanoscale. *Nanotechnology* **2016,** *27*, 315302.

59. Fenwick, O.; Bozec, L.; Credgington, D.; Hammiche, A.; Lazzerini, G. M.; Silberberg, Y. R.; Cacialli, F.,Thermochemical nanopatterning of organic semiconductors. *Nat. Nanotechnol.* **2009,** *4*, 664-668.

60. Lyuksyutov, S. F.; Vaia, R. A.; Paramonov, P. B.; Juhl, S.; Waterhouse, L.; Ralich, R. M.; Sigalov, G.; Sancaktar, E. Electrostatic Nanolithography in Polymers Using Atomic Force Microscopy. *Nat. Mater.* **2003,** *2*, 468-472.

61. Liu, G.-Y.; Xu, S.; Qian, Y.,Nanofabrication of Self-Assembled Monolayers Using Scanning Probe Lithography. *Acc. Chem. Res.* **2000,** *33*, 457-466.

62. Garno, J. C.; Yang, Y.; Amro, N. A.; Cruchon-Dupeyrat, S.; Chen, S.; Liu, G.-Y. Precise Positioning of Nanoparticles on Surfaces Using Scanning Probe Lithography. *Nano Lett.* **2003,** *3* , 389-395.

63. Moreno-Moreno, M.; Ares, P.; Moreno, C.; Zamora, F.; Gómez-Navarro, C.; Gómez-Herrero, J. AFM Manipulation of Gold Nanowires To Build Electrical Circuits. *Nano Lett.* **2019,** *19*, 5459-5468.

64. Headrick, J. E.; Armstrong, M.; Cratty, J.; Hammond, S.; Sheriff, B. A.; Berrie, C. L. Nanoscale Patterning of Alkyl Monolayers on Silicon Using the Atomic Force Microscope. *Langmuir* **2005,** *21*, 4117-4122.

65. Wendel, M.; Kühn, S.; Lorenz, H.; Kotthaus, J. P.; Holland, M., Nanolithography with an atomic force microscope for integrated fabrication of quantum electronic devices. *Appl. Phys. Lett.* **1994,** *65* (14), 1775-1777.

66. Wadu-Mesthrige, K.; Amro, N. A.; Garno, J. C.; Xu, S.; Liu, G.-Y. Fabrication of Nanometer-Sized Protein Patterns Using Atomic Force Microscopy and Selective Immobilization. *Biophys. J.* **2001,** *80*, 1891-1899.

67. Edwards, C. M.; Ulapane, S. B.; Kamathewatta, N. J. B.; Ashberry, H. M.; Berrie, C. L. Fabrication and Growth Control of Metal Nanostructures through Exploration of Atomic Force Microscopy-Based Patterning and Electroless Deposition Conditions. *J. Phys. Chem. C* **2020,** *124*, 25588-25601.

68. King, G. M.; Schürmann, G.; Branton, D.; Golovchenko, J. A. Nanometer Patterning with Ice. *Nano Lett.* **2005,** *5*, 1157-1160.

69. Yuan, M.; Zhan, S.; Zhou, X.; Liu, Y.; Feng, L.; Lin, Y.; Zhang, Z.; Hu, J. A Method for Removing Self-Assembled Monolayers on Gold. *Langmuir* **2008,** *24*, 8707-8710.

70. Frantz, P.; Granick, S. Surface Preparation of Silicon for Polymer Adsorption Studies. *Langmuir* **1992,** *8*, 1176-1182.

71. Guo, L.-H.; Facci, J. S.; McLendon, G.; Mosher, R. Effect of Gold Topography and Surface Pretreatment on the Self-Assembly of Alkanethiol Monolayers. *Langmuir* **1994,** *10*, 4588-4593.

72. Mantilaka, M. M. M. G. P. G.; Pitawala, H. M. T. G. A.; Rajapakse, R. M. G.; Karunaratne, D. G. G. P.; Upul Wijayantha, K. G. Formation of Hollow Bone-Like Morphology of Calcium Carbonate on Surfactant/Polymer Templates. *J. Cryst. Growth* **2014,** *392*, 52-59.

73. Mantilaka, M. M. M. G. P. G.; Karunaratne, D. G. G. P.; Rajapakse, R. M. G.; Pitawala, H. M. T. G. A. Precipitated Calcium Carbonate/Poly(Methyl Methacrylate) Nanocomposite Using Dolomite: Synthesis, Characterization and Properties. *Powder Technol.* **2013,** *235*, 628-632.

74. Babou-Kammoe, R.; Hamoudi, S.; Larachi, F.; Belkacemi, K. Synthesis of $CaCO_3$ Nanoparticles by Controlled Precipitation of Saturated Carbonate and Calcium Nitrate Aqueous Solutions. *Can. J. Chem. Eng.* **2012,** *90*, 26-33.

75. Deepika; Hait, S. K.; Christopher, J.; Chen, Y.; Hodgson, P.; Tuli, D. K. Preparation and Evaluation of Hydrophobically Modified Core Shell Calcium Carbonate Structure by Different Capping Agents. *Powder Technol.* **2013,** *235*, 581-589.

76. Liu, Z. H.; Brown, N. M. D.; McKinley, A. Evaluation of the Growth Behaviour of Gold Film Surfaces Evaporation-Deposited on Mica Under Different Conditions. *J. Phys.: Condens. Matter* **1997,** *9*, 59-71.

77. Levlin, M.; Laakso, A. Evaporation of silver Thin Films on Mica. *Appl. Surf. Sci.* **2001,** *171*, 257-264.

78. Nguyen, T. P.; Ip, J.; Le Rendu, P.; Lahmar, A. Improved Adhesion of Gold Coatings on Ceramic Substrates by Thermal Treatment. *Surf. Coat. Technol.* **2001,** *141*, 108-114.

79. Haahr, A.-M.; Jacobsen, C. Emulsifier Type, Metal Chelation and pH Affect Oxidative Stability of N-3-Enriched Emulsions. *Eur. J. Lipid Sci. Technol.* **2008,** *11*, 949-961.

80. Gulensoy, H.; Savci, H. Solubilities of Some Calcium Minerals and Prepared Calcium Compounds in EDTA (Ethylene Diamine Tetraacetic Acid) Solutions. *Maden Tetkik Arama Enst. Derg.* **1976,** *86*, 77-94.

81. Lee, D. K.; Kim, S.; Oh, S.; Choi, J.-Y.; Lee, J.-L.; Yu, H. K. Water-Soluble Epitaxial NaCl Thin Film for Fabrication of Flexible Devices. *Scientific Reports* **2017,** *7*, 8716.

82. Garno, J. C.; Batteas, J. D. Nanofabrication with Self-Assembled Monolayers by Scanning Probe Lithography. *Applied Scanning Probe Methods IV: Industrial Applications*, Bhushan, B.; Fuchs, H., Eds. Springer: Berlin Heidelberg, 2006; pp 105-135.

83. Fleischer, J.; Deuchert, M.; Ruhs, C.; Kühlewein, C.; Halvadjiysky, G.; Schmidt, C. Design and Manufacturing of Micro Milling Tools. *Microsyst. Technol.* **2008,** *14*, 1771-1775.

84. Böhme, G.; Hohn, P.; Krupp, H.; Rabenhorst, H.; Schnabel, W.; Walter, G. Adhesion of Gold Particles to Silicon and Gold Substrates in Ultrahigh Vacuum. *J. Appl. Phys.* **1973,** *44*, 3914-3918.

TOC Graphic

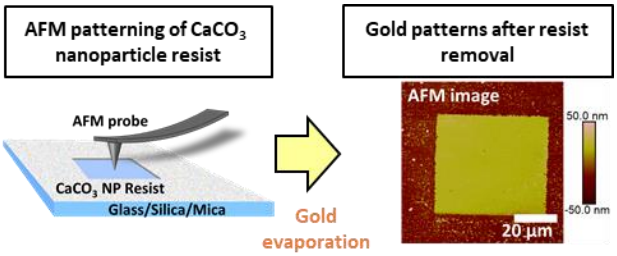
AFM patterning of $CaCO_3$ nanoparticle resist
Gold patterns after resist removal
AFM probe
$CaCO_3$ NP Resist
Glass/Silica/Mica
Gold evaporation
AFM image
50.0 nm
-50.0 nm
20 µm